Experimental report for expt no. CH4680

Studying inorganic chemistry in nano test-tubes: Elucidating the formation mechanism of nanomaterials using in situ NEXAFS spectroscopy

Introduction

Metal nanoparticles (MNPs) have attracted considerable interest recently due to their applications in catalysis and sensing.[1-4] In order to comprehensively unlock the potential of these materials, it is important to fully understand how they form. Due to advances in aberration-corrected high resolution transmission electron microscopy (AC-HRTEM), it is possible to not only view nano-sized materials in direct space and real time, but also apply energy and initiate chemical transformations, such as the formation of highly crystalline platinum nanoparticles from amorphous platinum, or the breakage of a SWNT sidewall catalysed by encapsulated nickel nanoparticles. Prolonged irradiation of a sample by electron beam irradiation results in the displacement of carbon atoms and bond dissociations, leading to the gradual destruction of the sample being analysed which is a generally undesirable process.[5-7] Therefore, whilst it is possible to monitor inorganic transformations using AC-HRTEM, electron microscopy is an invasive analytical technique which can perturb the intrinsic structures of materials and mask chemical transformations.

Fluorescence-detected X-ray absorption spectroscopy (FD-XAS) can be employed as a technique to characterise nanomaterials by probing amongst other qualities, the oxidation state of materials, and so can be used as a method of discriminating between the encapsulated precursors and the product formed upon their heating.[8, 9] This is possible since the shape and magnitude of the spectral features from each compound are different, which corresponds to variations in the oxidation states of the materials.[10] Notably, unlike AC-HRTEM, it is a bulk technique which involves exposing a sample to X-rays, over an area typically on the order of mm^2, and so is also non-destructive at the conditions required for obtaining data. This is advantageous as it allows the material to then be retained for further analysis.

As well as using this technique to characterise materials statically, it is also possible to form a material, apply an external stimulus such as heat, and perform FD-XAS *in-situ*. Subsequently, time resolved FD-XAS is an appropriate technique for obtaining information on the formation mechanisms of MNPs. For example, the nucleation process of AuNPs has been investigated by Wai *et al.* using *in-situ* XAS and allowed for the proposal of a detailed reaction mechanism, as intermediates were detected-.[11] Additionally, Ohyama *et al*. showed how the formation of AuNPs is affected by the presence of dodecanethiol and a catalytic activity dependence on the size of AuNPs was observed.[12] More recently, Jiang *et al*. have demonstrated that the reduction of Pt^{4+} ions can be investigated using the same technique,[13] and so observing how the edge energies of each material change as a function of

temperature should allow for a detailed explanation of the properties of each transformation.

Carbon nanostructures such as single-walled carbon nanotubes (SWNTs), are extremely interesting as they contain distinctive nanoscale channels which can be filled with a variety of different materials including inorganic salts,[14-16] organic molecules,[17, 18] and metallic nanoparticles.[19-21] The mechanical, chemical and physical properties of MNPs can be altered upon encapsulation into SWNTs which can lead to changes in catalytic activity, as is observed for the synthesis of ammonia catalysed by ruthenium nanoparticles.[22] Furthermore, the stability of platinum nanoparticles can be improved upon encapsulation into carbon nanostructures which in turn could lead to a decrease in platinum consumption for catalytic processes.[23] Not only can SWNTs act as sheaths to improve the efficiency of MNPs, their unique one-dimensional channel allows them to act as nano test tubes which ensures that the analysis and reaction of encapsulated molecules can be done with ease.

We have observed previously that the thermal treatment of $Cu(acac)_2$@SWNT leads to the formation of Cu_2O_x@SWNT, whereas the thermal treatment of $Pt(acac)_2$@SWNT leads to the formation of Pt@SWNT. When observed at static temperatures, the $M(acac)_2$@SWNT (M= Cu, Pt) precursors have many noticeable differences to their respective products, with changes in their electronic properties, physical morphology and chemical properties all being observed. Herein, the formation of Cu_2O_x@SWNT from $Cu(acac)_2$@SWNT, and Pt@SWNT from $Pt(acac)_2$@SWNT has been investigated using FD-XAS, and this has allowed for the precise temperature of each respective transformation to be determined.

Results and Discussion

Ex-situ Decomposition of $Cu(acac)_2$@SWNT to Cu_2O_x@SWNT

$Cu(acac)_2$@SWNT (figure 1 a) can be heated under an inert atmosphere at 500 ^oC to form Cu_2O_x@SWNT (figure 1 b, scheme 1), where $x > 1$.

Raman spectroscopy reveals a large blue shift in the position of the G band of Cu_2O_x@SWNT relative to an empty SWNT and $Cu(acac)_2$@SWNT (+11 cm^{-1}), (figure 2), indicating charge transfer from the SWNT to the encapsulated material.[24] The model of Cu_2O@SWNT (figure 1 b) shows an excess of oxygen atoms in the material, and so it is probable that the resultant structure has a slight negative charge, which results in a transfer of electron density being observed from the nanotube and hence the blue shift of the G band.[25]

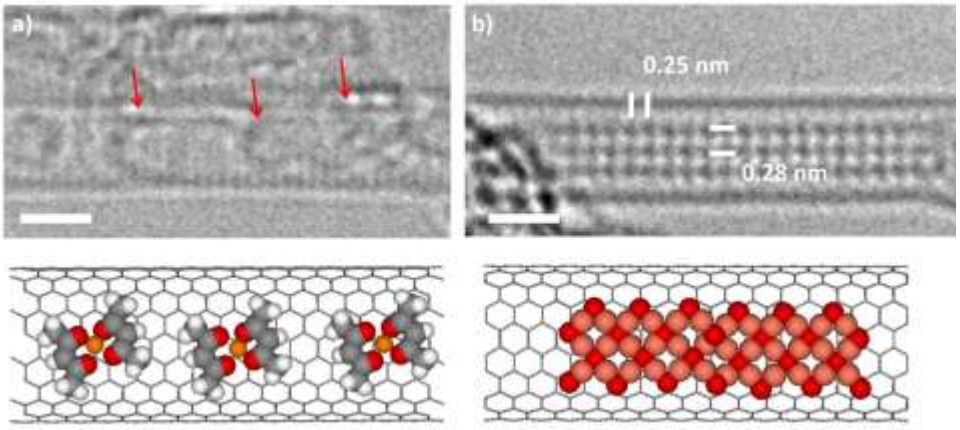

Figure 1: AC-HRTEM images showing a) $Cu(acac)_2$@SWNT, the darker contrast features (red arrows) are copper, whereas the lighter contrast material is a mixture of adventitious carbon and remnants of the acetylacetonate ligand which is decomposing under the electron beam; b), Cu_2O_x@SWNT. The structure adopts a highly crystalline cubic arrangement. The scale bars are 0.5 nm and below each AC-HRTEM image is a geometry optimised model of the structures in a (10,10) SWNT.

$$Cu(acac)_2 + SWNT \xrightarrow[3\ days,\ 10^{-5}\ mbar]{110\ ^oC} Cu(acac)_2@SWNT \xrightarrow[1\ hr,\ Ar]{500\ ^oC} [Cu_2O_x]^{((x-1).2)-}@SWNT^{((x-1).2)+}$$

Scheme 1: The formation of Cu_2O_x@SWNT, by first encapsulating $Cu(acac)_2$ into SWNTs and then heating.

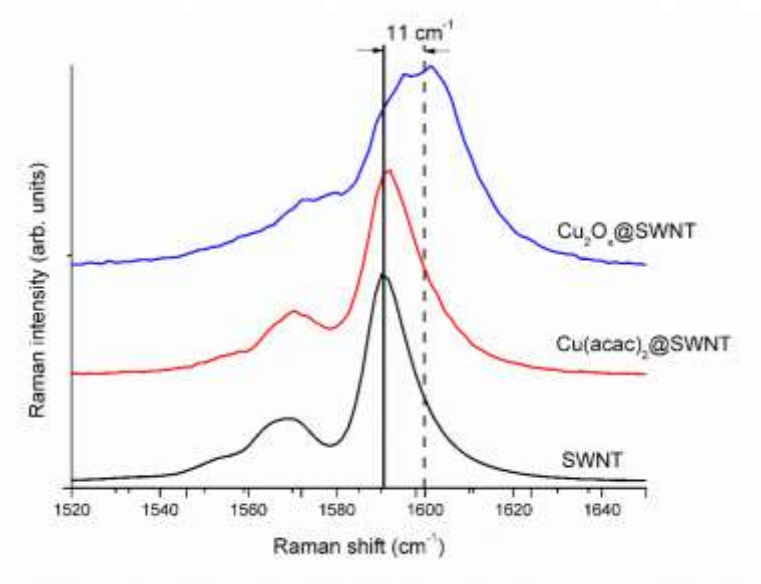

Figure 2: Raman spectra focussing on the G band of Cu_2O_x@SWNT (blue) and $Cu(acac)_2$@SWNT (red) compared to an empty SWNT (back). Whilst there is a negligible shift in the G band spectra of $Cu(acac)_2$@SWNT relative to empty SWNTs, the position of the G band of Cu_2O_x@SWNT sample increases significantly (+11 cm^{-1}).

FD-XAS was recorded for both materials. The energy of the copper K edge of both materials was taken, and compared to the copper K edge of a variety of standards (table 1).

Table 1: Copper K edge energy of $Cu(acac)_2$@SWNT, Cu_2O_x@SWNT, and known standards relative to copper metal.

Material	Formal Cu oxidation state	Cu K edge (eV)	Difference from Cu K edge of Cu(0) (eV)
Cu	0	8975.53 ± 0.079	**0**
Cu_2O_x@SWNT	1	8980.42 ± 0.037	**4.89**
$Cu(CO_2CH_3)$	1	8982.18 ±0.061	**6.65**
$Cu(acac)_2$	2	8984.76 ± 0.370	**9.23**
$Cu(acac)_2$@SWNT	2	8986.76 ± 0.093	**11.23**

An increase in the K edge energy of copper in $Cu(acac)_2$@SWNT is observed relative to the unencapsulated material which suggests a decrease of electron density on the copper centre when the complex is encapsulated. As the Raman data does not show any significant change in the G band of the SWNT for $Cu(acac)_2$@SWNT, this demonstrates that any charge transfer that takes place in this material occurs only in the complex itself, and does not involve the SWNT. Since FD-XAS shows a decrease of electron density on the copper atom upon encapsulation, it is proposed that the nanotube has acted to polarise the Cu-O bonds, resulting in greater shift of electron density from the Cu atom to O atoms, such that the Cu-O bond becomes more ionic (figure 3 a).

Upon heating to 500 ^oC a significant decrease in the energy of the copper K edge from $Cu(acac)_2$@SWNT to Cu_2O_x@SWNT occurs which indicates that the copper centre has gained electron density. The energy is similar to that of a known Cu(I) complex, copper (I) acetate, but is slightly lower, and is therefore is consistent with the formation of a Cu(I) species, but with electron density being transferred from the nanotube to the guest compound (figure 3 b).

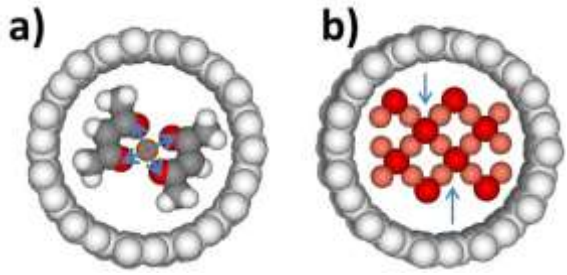

Figure 3: Models of (a) $Cu(acac)_2$@SWNT and (b) Cu_2O_x@SWNT showing charge transfers taking place within the guest species (blue arrows depict the flow of negative charge). With $Cu(acac)_2$@SWNT electron density is shifted further from the copper atom to oxygen atoms resulting in the polarisation of the bonds, whereas for Cu_2O_x@SWNT, negative charge is transferred from the nanotube wall to the guest material.

Not only are the positions of the copper K edge of $Cu(acac)_2$@SWNT and Cu_2O_x@SWNT significantly different, their shapes also vary. While the FD-XAS of $Cu(acac)_2$@SWNT shows a sharp transition between 8.972 to 8.993 keV (figure 4 a), the spectrum for Cu_2O_x@SWNT has a slightly broader range (8.969 to 8.992 keV) with a distinct feature at 8.98k eV (figure 4 b). All of the spectra were smoothed using Matlab, and figure 4 gives an example of how accurate the smoothing was. The points represent the raw data, and the black line shows the curves produced as a result of the smoothing.

Attempted Monitoring of the Shift with *in-situ* Heating

Clearly, the AC-HRTEM images of $Cu(acac)_2$@SWNT before and after heat treatment demonstrate that different materials are present inside the nanotube, and this is supported by both the Raman and FD-XAS data which show changes in electronic states of the SWNT and guest compound upon heating. Therefore the sample was heated slowly, and systematically monitored using FD-XAS to investigate whether the precise transition could be observed.

The encapsulated metallic precursor $Cu(acac)_2$@SWNT (5 mg) was placed in a glass capillary tube and held in position with glass wool (figure 5 a.1). The tube was placed within an aluminium frame, and sealed in place using wax, to ensure no air could enter the system. The frame was then placed in position above a heater (figure 5 a.4) and attached to a helium source (in figure 5 a.2, out figure 5 a.3, flow rate *ca.* 30 mL/min), and the system was purged with helium for 15 min to ensure all air was removed from the capillary tube. Finally, the system was heated rapidly (at a rate of 50 ^{o}C/s) which allowed for precise control of temperature when needed.

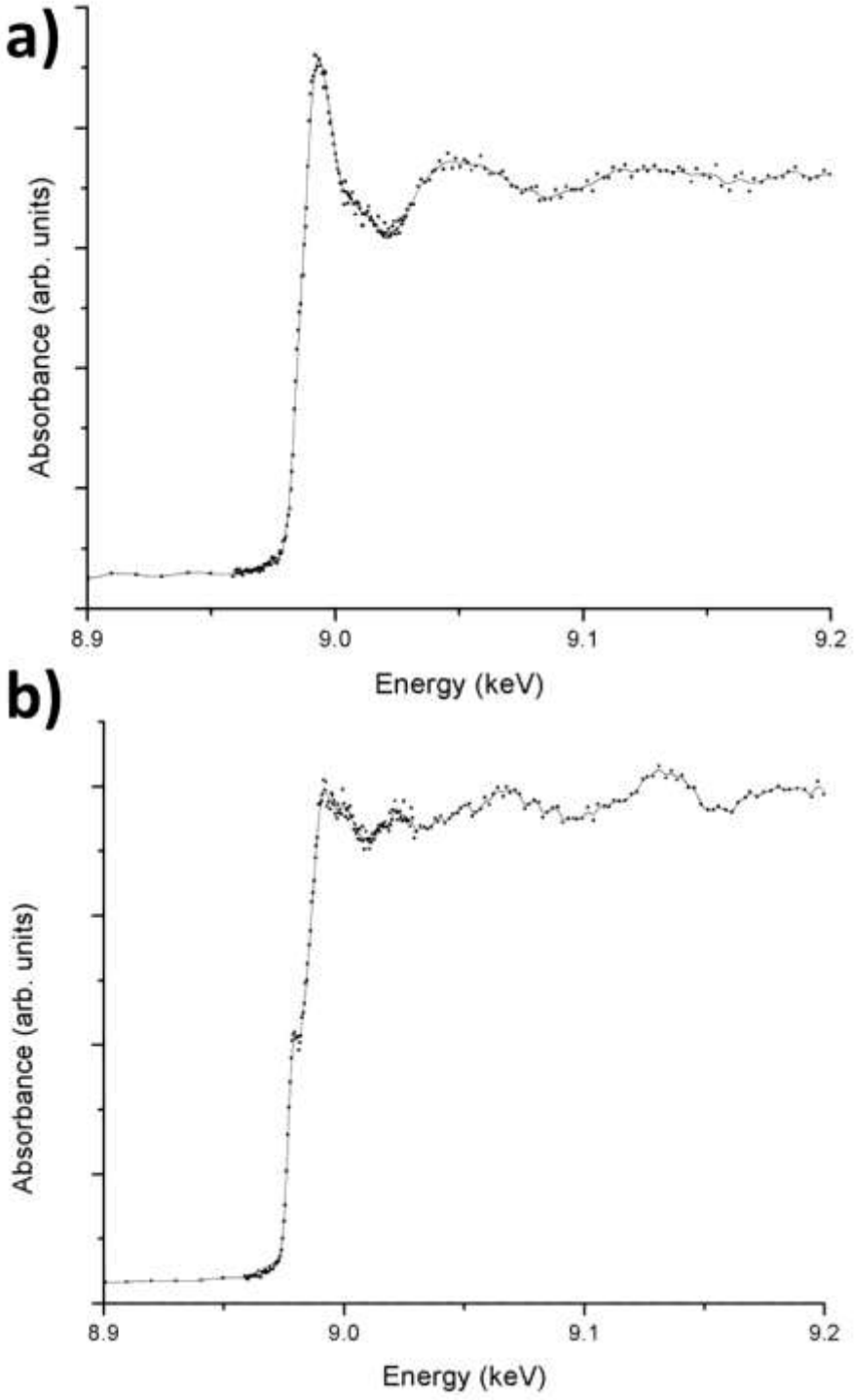

Figure 4: FD-XAS of (a) $Cu(acac)_2$@SWNT and (b) Cu_2O_x@SWNT. The Cu_2O_x@SWNT was formed *ex-situ* and both spectra were recorded at room temperature. The shape of the two spectra are noticeably different, with an extra feature observed at 8.98 keV for the spectrum of Cu_2O_x@SWNT.

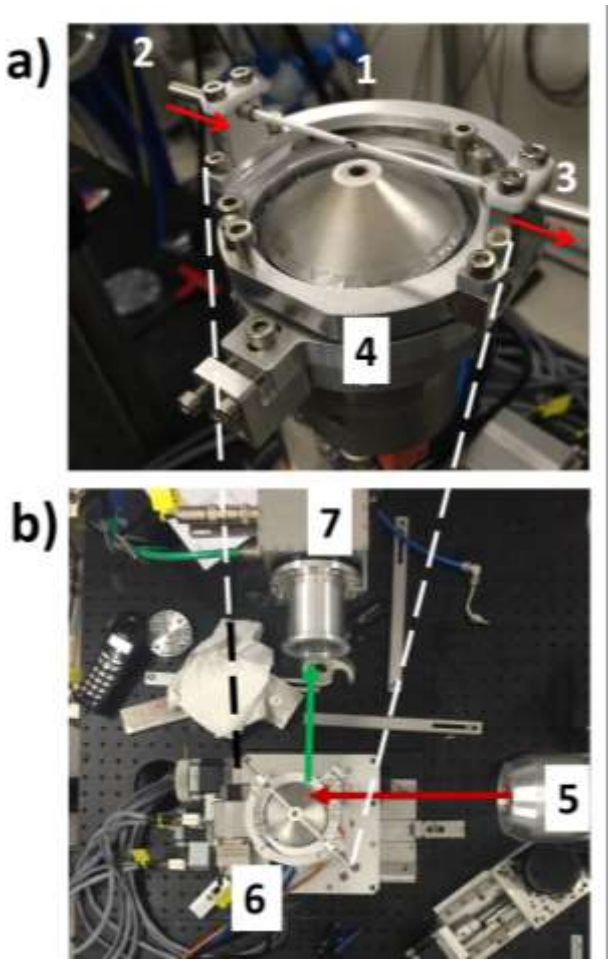

Figure 5: Photographs from the ESRF showing a) how the sample of $Cu(acac)_2$@SWNT was prepared for the heating experiment. A small amount of $Cu(acac)_2$@SWNT was placed in a glass capillary tube (1), which was placed in a steel frame and mounted above a heat source (4). A helium gas flow was attached (2), to purge the system of air and provide an inert atmosphere; b) the position of the X-ray source (5) relative to the sample (6) and fluorescence detector, (7). The red arrow represents the flow of X-rays, and the green arrow shows the fluorescence signal, which is detected perpendicular to the X-ray source.

Initially, a spectrum of $Cu(acac)_2$@SWNT was recorded at room temperature and the sample was heated to 100 ^oC (at a rate of 50 $^oC/s$), held at this temperature for 5 min and another spectrum was recorded. X-rays (figure 5 b.5, red arrow) were tuned to the required energy for the copper K edge (8.988 keV) and travelled through the sample (figure 5 b.6) and X-ray fluorescence (green arrow) was detected perpendicularly (figure 5 b.7).

After obtaining a spectrum of the sample at 100 ^oC, which took approximately 8 min, the temperature of the arrangement was increased from 100 ^oC to 125 ^oC, held for 5 min and a subsequent spectra recorded, the scan took approximately 8 min and this process continued in 25 ^oC steps until there was no further change in the energy of the edge position. $Cu(acac)_2$@SWNT was consequently heated to 300 ^oC over *ca.*

120 min. Each spectrum was smoothed using a Matlab function, and all spectra were collated and compared with that of Cu_2O_x@SWNT formed *ex-situ* (figure 6)

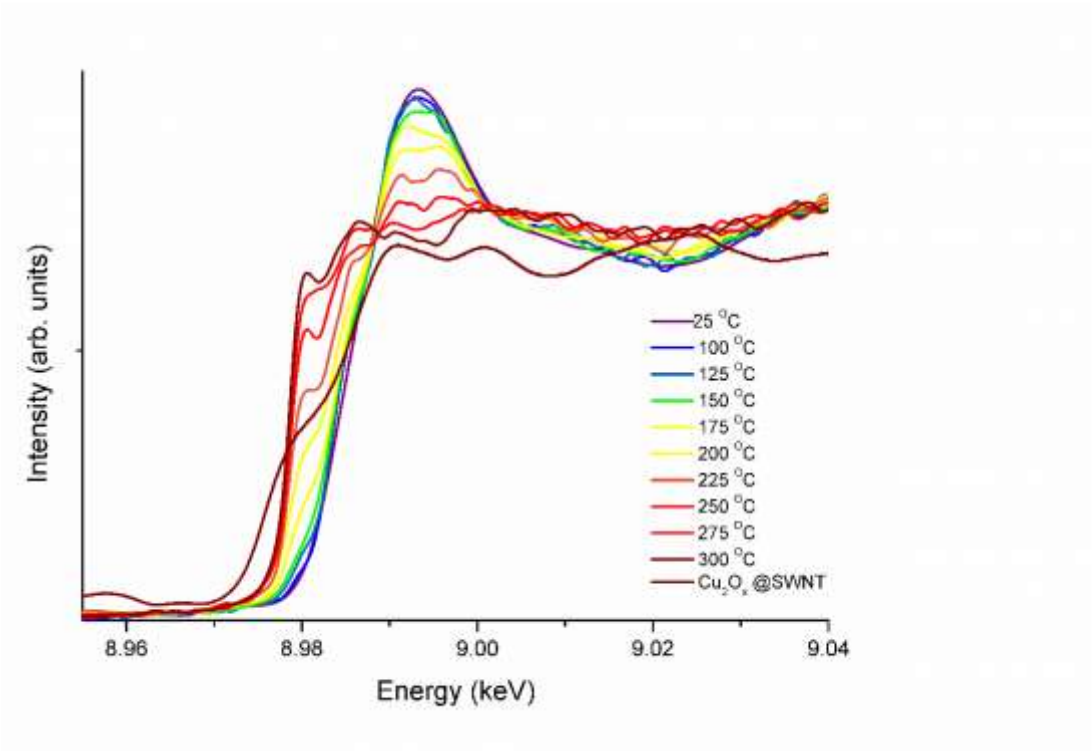

Figure 6: FD-XAS obtained for $Cu(acac)_2$@SWNT at 25 °C (purple line), then heated to 100 °C (blue) followed by subsequent heating at 25 °C increments. As the temperature increases, the shape of each spectrum changes, and gradually appears to resemble that of Cu_2O_x@SWNT formed *ex-situ*.

When the edge region of all the spectra are closely examined (figure 7), it is clear that the energy of the edge decreases as a function of temperature (figure 7 a). The first derivative of the edge position at each temperature has been shown which allows for the exact position of the energy to be recorded (figure 5.7 b), and at temperatures below 175 °C, the edge occurs at around 8.9889 keV; however, when heated to 175 °C, there is a decrease of around 5 eV to 8.9838 keV. After further heating to 200 °C the edge decreases by another 5 eV to 8.9787 keV.

The sample was further heated to 300 °C, but no additional shift in the energy of the edge was observed. Since the energy of the copper K edge of $Cu(acac)_2$@SWNT (8.9867 keV) has a standard deviation of 0.0183 eV, and the copper K edge of Cu_2O_x@SWNT (8.9763 keV) has a standard deviation of 0.0933 eV, a change of 10 eV is clearly significant. This experiment has shown that the edge energy of $Cu(acac)_2$@SWNT decreases as a function of temperature and is only 2eV greater than the edge position of Cu_2O_x@SWNT formed *ex-situ*.

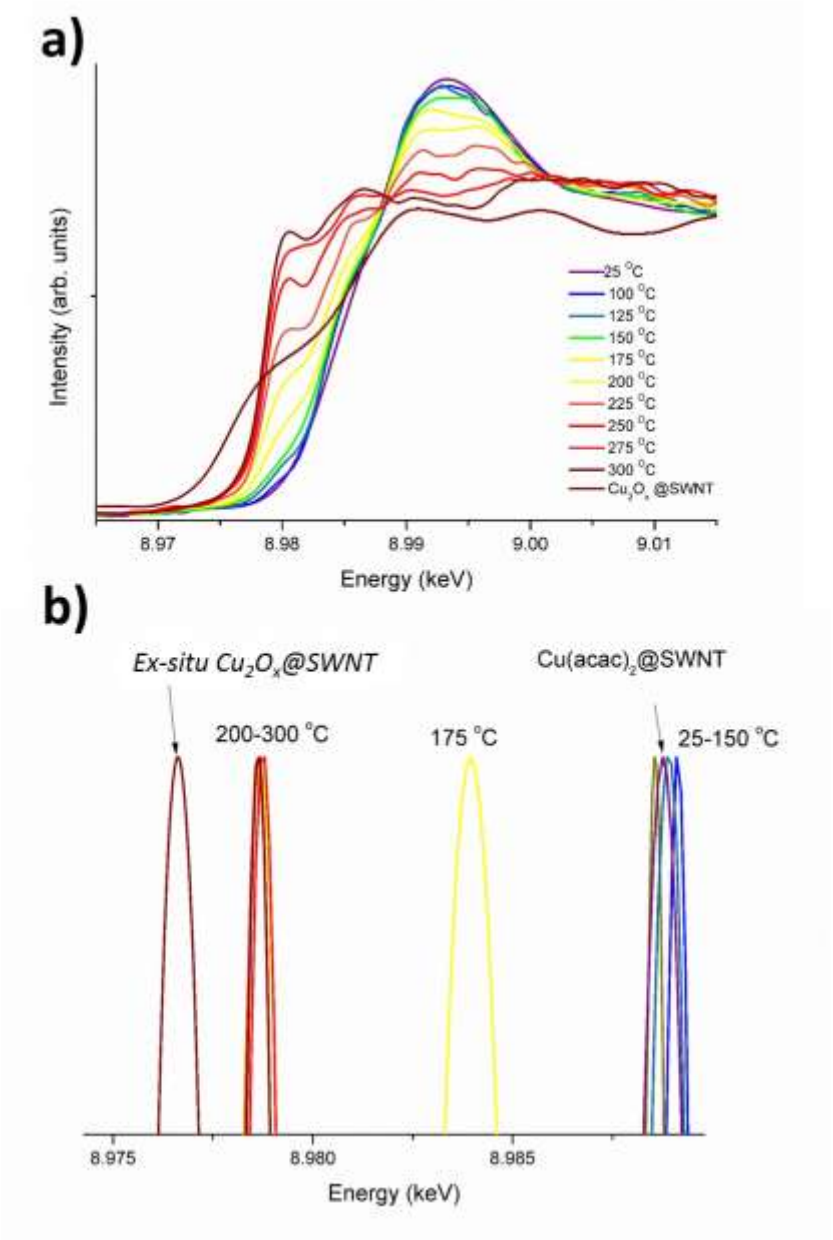

Figure 7: The specta from figure 5.6, zoomed in to show how the position of the edge changes as a function of temperature. There is a significant decrease in the position of the edge (*ca.* 5 eV) at 175 °C, which is depicted by the first derivatives of each edge (b).

As shown by the first derivative plots of each spectrum (figure 7 b), the position of the edge decreased after 175 °C. The values before 175 °C are typical of that of $Cu(acac)_2$@SWNT, whereas the data obtained at higher temperatures is more indicative of the formation of a reduced copper species, and is similar to that of Cu_2O_x@SWNT formed *ex-situ*. Figure 5.8 shows how the energy of the Cu edge varies as a function of temperature, with the energy positions of Cu_2O_x@SWNT formed *ex-situ* and monitored at 25 °C and 300 °C shown for reference (red squares).

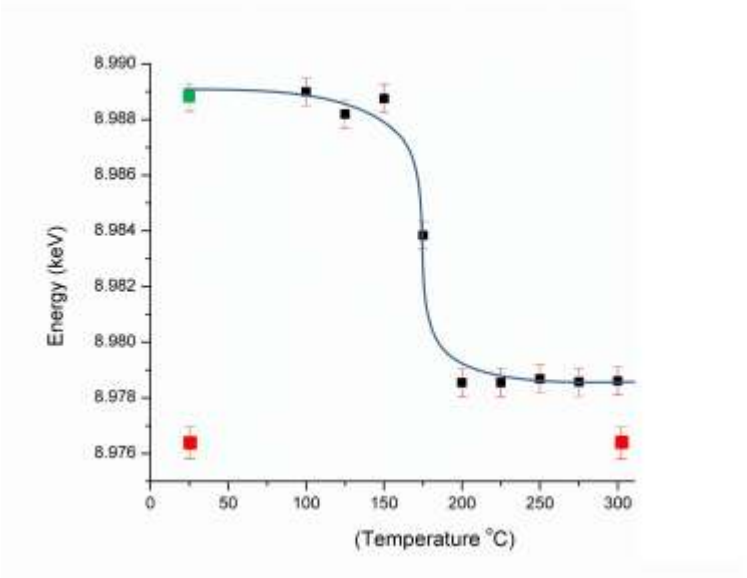

Figure 8: A plot showing how the energy of the copper K edge in $Cu(acac)_2$@SWNT changes as a function of temperature. Between the starting temperature of 25 °C (green square) and 150 °C the edge energy remains around 8.988 keV, followed by a significant decrease in the edge energy around 175 °C. After 200 °C the position of the edge stabilises at around 8.9784 keV, which is a similar energy to the edge positions of Cu_2O_x@SWNT formed *ex-situ* (red squares).

Since the heat dependent FD-XAS showed that a significant decrease in the edge energy occurs around 175 °C, an additional sample of $Cu(acac)_2$@SWNT was prepared and heated at 175 °C for 1 hr and the edge energy constantly monitored (figure 9 a). The energy the edges were compared to the edge of $Cu(acac)_2$ at 25 °C (green square) and Cu_2O_x@SWNT formed *ex-situ* (red line figure 9 a). It is important to note that as a control, Cu_2O_x@SWNT formed *ex-situ* was monitored at both 25 °C and 300 °C to ascertain whether the edge is affected by temperature change, and no change was observed, and consequently is assumed to remain constant with temperature. It was envisaged that holding the sample at a temperature around the experimentally obtained transition point should allow for a very gradual change to be observed. After the first spectrum was recorded at 175 °C, a process which took 8 min, a decrease of 8 eV in the edge energy was observed, and after prolonged heating no further change was observed.

Monitoring how the edge energy changes when held around the temperature of formation allowed for detailed kinetic behaviour to be observed. By comparing how close the values obtained were when $Cu(acac)_2$@SWNT was held at 175 °C, to $Cu(acac)_2$ at 25 °C and Cu_2O_x@SWNT formed *ex-situ*, it is possible to evaluate how far the reaction has completed. If the edge obtained for Cu_2O_x@SWNT (8.9763 keV) represents 100% conversion, and the values for the edge of $Cu(acac)_2$@SWNT obtained at 25 °C represents 0% conversion, the first value obtained from heating

$Cu(acac)_2$@SWNT to 175 °C (*ca.* 8.9784 keV) represents 80% conversion, and the subsequent energies also hover around this point, implying no further reaction at 175 °C (figure 9 b). Therefore the rate of transformation is too fast and takes place on a time scale quicker than FD-XAS measurements.

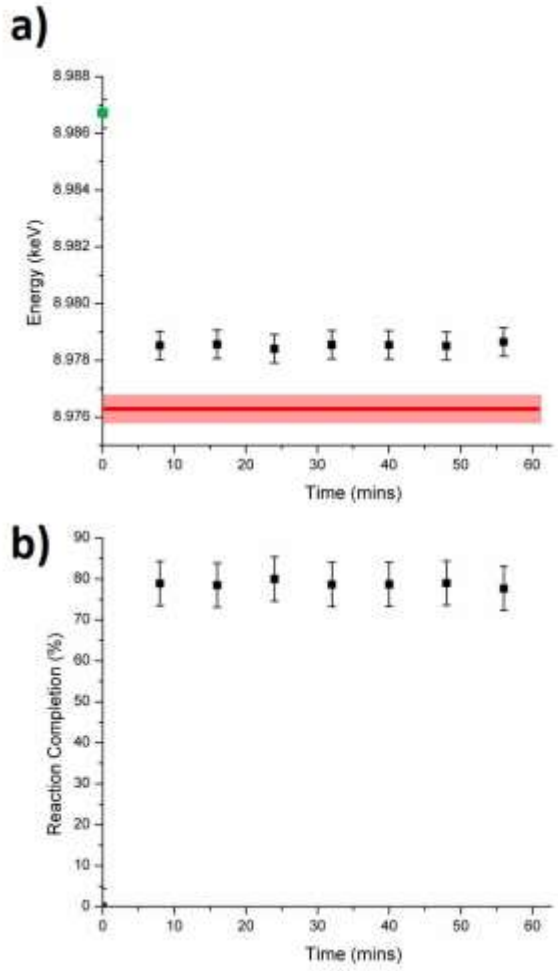

Figure 9: a) A plot showing how the edge energy changes when $Cu(acac)_2$@SWNT is heated at 175 °C for 1 hr. Initially there is a decrease (8 eV) from that of $Cu(acac)_2$@SWNT at 25 °C (green square), but over time, there is no significant difference at 175 °C, and all values remain within 0.3 eV of each other. The edge energy of Cu_2O_x@SWNT formed *ex-situ* is shown for comparison (red line); b) A plot showing the reaction completion of $Cu(acac)_2$@SWNT to Cu_2O_x@SWNT as a function of time. After heating $Cu(acac)_2$@SWNT from 25 °C to 175 °C, the reaction rapidly takes place and a rate of 80% conversion to Cu_2O_x@SWNT is observed.

$Cu(acac)_2$@SWNT has been heated to form Cu_2O_x@SWNT, and the changes monitored using FD-XAS. It has been shown that the transition occurs rapidly at around 175 °C which is a significantly lower temperature than that for bulk $Cu(acac)_2$ which shows that encapsulation within the hollow channel of the SWNT lowers the activation energy (E_a) needed for the reaction.[26] By comparing data obtained from

the FD-XAS of $Cu(acac)_2$@SWNT with bulk $Cu(acac)_2$, a decrease of electron density on the copper is observed upon encapsulation which is caused by the Cu-O bonds being polarised which weakens the bonding and subsequently lowers the energy required. Confinement into a SWNT lowers the activation barrier of transformations since van der Waals interactions polarising the bonds reduce the bond enthalpy (figure 10), and so less energy is required to transform $Cu(acac)_2$@SWNT into Cu_2O_x@SWNT.[27]

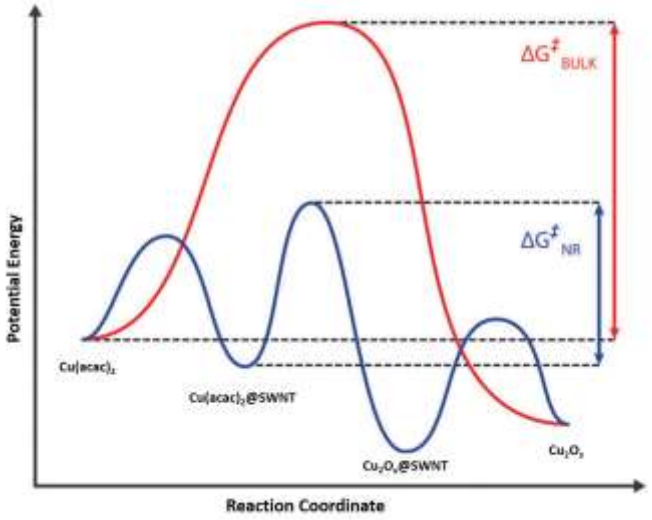

Figure 10: A reaction energy profile hypothetically comparing the formation of Cu_2O_x@SWNT from $Cu(acac)_2$@SWNT. Although there are more stages due to the necessary encapsulation and release of products, the stabilisation of the transition state *via* van der Waals forces can reduce the activation energy necessary for the reaction to proceed. Adapted from Miners *et al.*, 2016.[28]

$Cu(acac)_2$@SWNT was further heated to 500 ^{o}C to completely replicate the *ex-situ* experiment, and the position of the copper K edge was monitored; however, no further change in the shape of the edge, or position was found to occur, and so the energy of the edge and shape of the spectrum never fully reaches the position for Cu_2O_x@SWNT formed *ex-situ*. This could be caused by the ability of the nanotube to stabilise the charge of the formed species, *i.e.* it is possible that this sample has a higher loading of material that the sample formed *ex-situ*, and so the nanotube is physically unable to transfer anymore charge, therefore this needs to be investigated further.

Transformation of $Pt(acac)_2$@SWNT to Pt@SWNT

In addition to copper, platinum has attracted significant interest due to its applications in catalysis and sensing.[4, 29-31] However, unlike $Cu(acac)_2$@SWNT, when $Pt(acac)_2$@SWNT is heated to 500 ^{o}C in an inert atmosphere, platinum nanoparticles form, with no oxide present (Scheme 2).

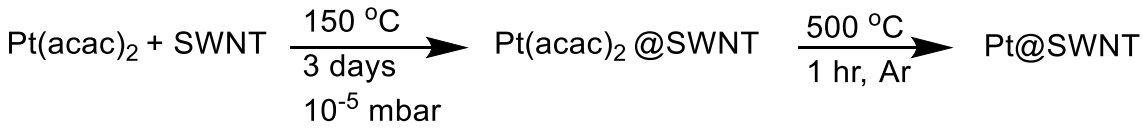

Scheme 2: The formation of Pt@SWNT from the encapsulation and subsequent heating of $Pt(acac)_2$.

AC-HRTEM analysis of $Pt(acac)_2$@SWNT shows discrete clusters of complex (figure 11 a). Upon heating the sample at 500 °C, the volatile acetylacetonate ligands are removed from the platinum, leading to the formation of a metallic structure (figure 11 b).

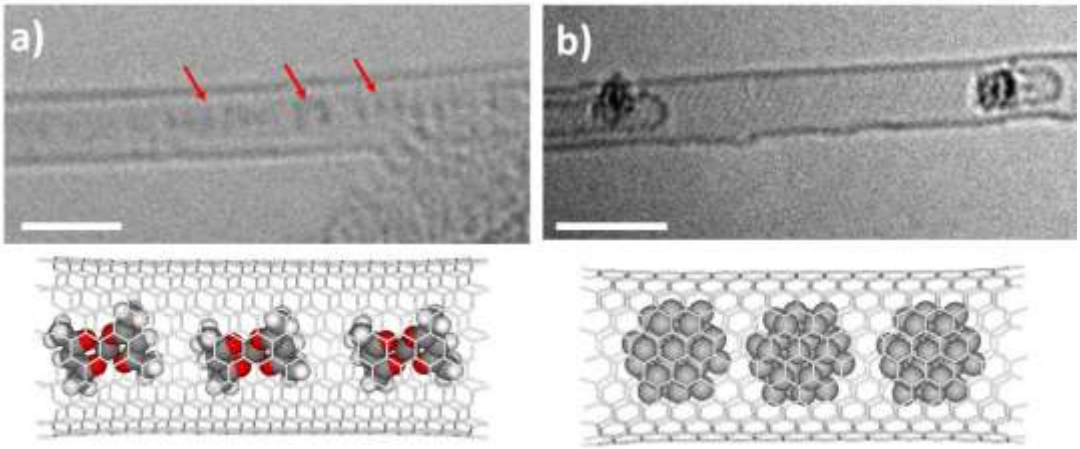

Figure 11: AC-HRTEM images of a) $Pt(acac)_2$@SWNT, the red arrows show the platinum atoms, and b) Pt@SWNT. The scale bars are 2 nm. Below each AC-HRTEM image is a geometry optimised model of each structure in a (10,10) SWNT.

Raman spectroscopy has been performed on $Pt(acac)_2$@SWNTs and Pt@SWNT (figure 12), with attention being placed on the G band of the structures, relative to empty SWNTs. Whilst there is only a negligible change in the position of the G band upon the encapsulation of $Pt(acac)_2$, upon thermal decomposition to Pt@SWNT, the G band red shifts by 4 cm^{-1} which is indicative of an electron transfer from the Pt to the SWNT, which is opposite to the shift observed for Cu_2O_x@SWNT.

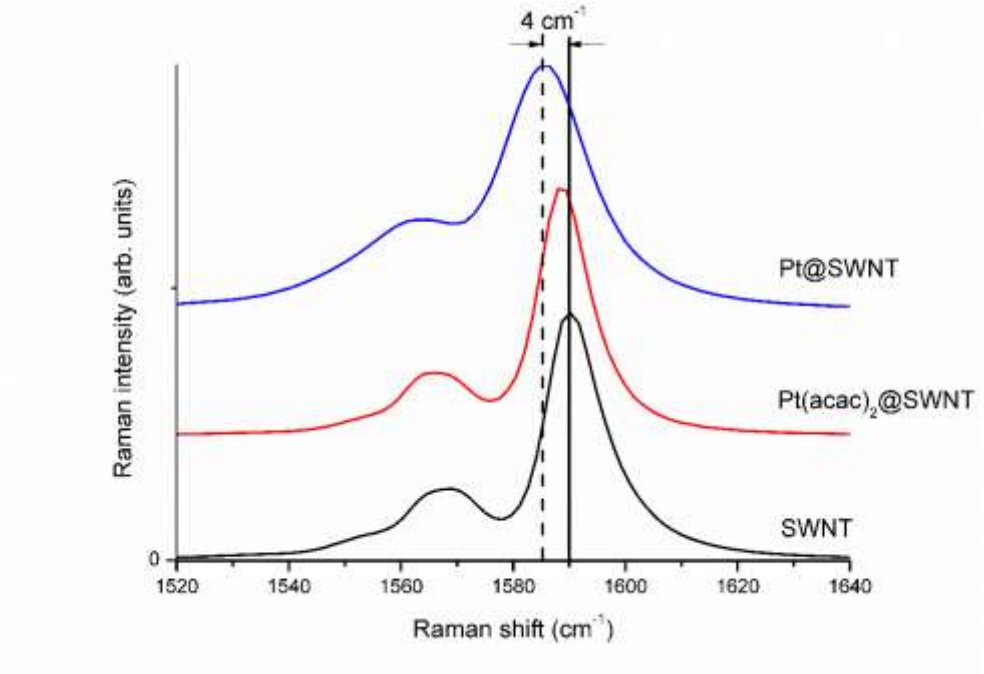

Figure 12: Raman spectra showing how the G band of the nanotube shifts depending on the encapsulated material. The encapsulation of $Pt(acac)_2$@SWNT leads to a negligible change in the position in the G band of the SWNT compared to empty SWNTs, and upon thermal decomposition the position of the G band decreases more significantly (4 cm^{-1}).

There is an increase in the energy of the platinum L_{III} edge of $Pt(acac)_2$ upon its encapsulation into SWNTs which is similar to the increase in the copper K edge observed upon encapsulation of $Cu(acac)_2$@SWNT. An increase of 1.48 eV occurs (table 2), which although seems small is significant given the small standard deviations of each sample. Again, this increase in edge energy, complimented by no change in the G band of the SWNT being observed in Raman, is attributed to the SWNT polarising the Pt-O bonds in the $Pt(acac)_2$ complex (figure 13).

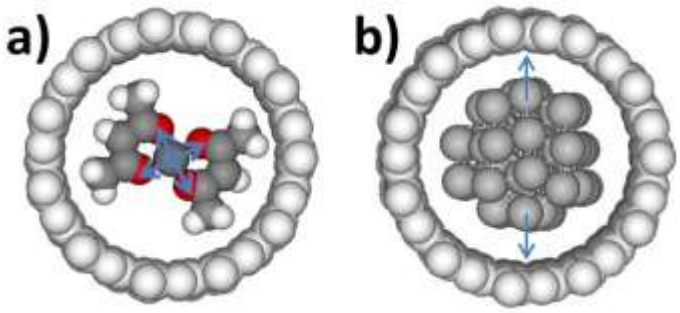

Figure 13: models of $Pt(acac)_2$@SWNT (a) and Pt@SWNT (b) showing electron transfers taking place within the materials (blue arrow depicts flow of electron charge). For $Pt(acac)_2$@SWNT electron density is being shifted from the platinum atom to oxygen atoms which results in the polarisation of the bonds, whereas for Pt@SWNT, electron density is being transferred from the platinum to the carbon atoms of the nanotube wall.

Table 2: Platinum L_{III} edge energy of $Pt(acac)_2$, $Pt(acac)_2$@SWNT and Pt@SWNT, compared to known standards and relative to Pt metal.

Sample	Formal Pt oxidation state	Pt L_{III} edge (eV)		Energy difference from Pt (eV)
Pt	0	11554.98	± 0.239	0
$Pt(acac)_2$	2	11556.08	± 0.045	1.10
Pt@SWNT	0	11556.24	± 0.002	1.26
PtI_2	2	11556.99	± 0.050	2.01
$Pt(acac)_2$@SWNT	2	11557.56	± 0.021	2.58

Upon thermal decomposition to form Pt@SWNT, the edge energy decreases by *ca.* 1.32 eV to 11556.24 eV (figure 14), which, again, although much smaller than the change which occurred for the copper K edge, is significant given the standard deviation for each material. Although the formation of platinum leads to a decrease in the edge energy, it is still significantly higher (1.26 eV) than the edge of bulk platinum which suggests a decrease of electron density on the platinum. This is complimented by the Raman data which shows a decrease in the G band suggesting charge has been transferred from platinum to the SWNT. Such electron transfers from encapsulated MNPs to SWNT are not uncommon, and have been reported for many encapsulated metal nanoparticles such as europium and erbium.[32, 33]

Attempted Monitoring of the Shift with *in-situ* Heating

In a similar method to the investigation of $Cu(acac)_2$@SWNT, $Pt(acac)_2$@SWNT was heated up from 100 ^oC to 350 ^oC in an inert atmosphere. An FD-XAS was recorded at 25 ^oC intervals, and the platinum edge energy monitored at these temperatures, with the whole heating taking approximately 2 hr (figure 15). Similarly to the *in-situ* heating of $Cu(acac)_2$@SWNT, the edge generally decreases; however, not as sharply.

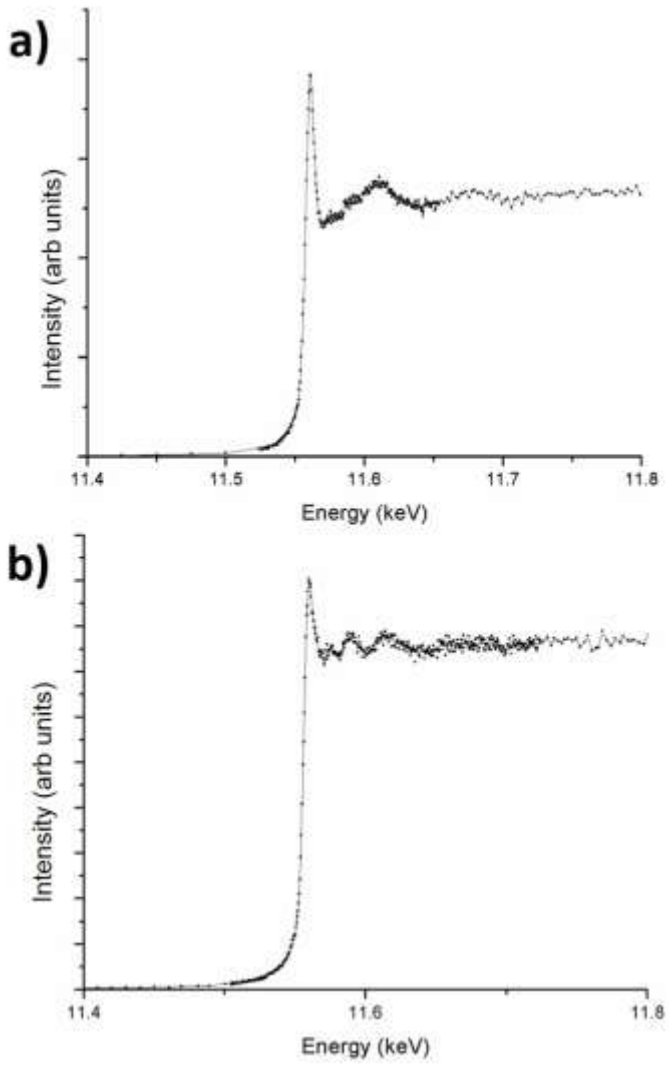

Figure 14: FD-XAS of (a) $Pt(acac)_2$@SWNT and Pt@SWNT (b). Both samples were recorded at room temperature, and there is a decrease in the position of the platinum L_{III} edge after thermal decomposition

Although the position of the edge inflections are all quite similar in value (figure 16 a), the first derivative has been taken of each edge (figure 16 b) and these show a gradual decrease in the position of the edge.

In contrast to the heating of $Cu(acac)_2$@SWNT, the change in the edge energy as a function of temperature is much more gradual (figure 17). The energy remains constant at 100 ^oC, decreases linearly between 100 and 175 ^oC, then remains constantly around 11557.0 keV before decreasing further after 275 ^oC. Eventually, the edge approaches that of Pt@SWNT formed *ex-situ*, 11556.24 eV, as shown by the red squares.

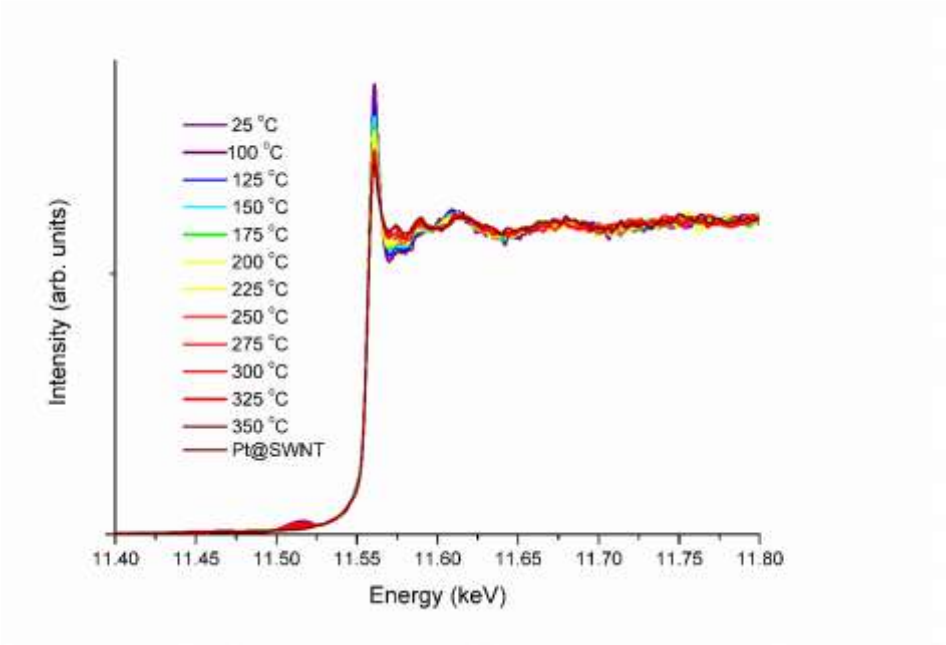

Figure 15: FD-XAS obtained for $Pt(acac)_2$@SWNT at 25 °C (purple line), then heated to 100 °C (blue) followed by subsequent heating at 25 °C intervals. As the temperature increases, the morphology of each spectra changes, and gradually appears to resemble that of Pt@SWNT formed *ex-situ*.

Similarly to the decomposition of $Cu(acac)_2$@SWNT, there is a decrease in the edge energy position (1.4 eV) upon heating, which is comparable to the difference observed between $Pt(acac)_2$@SWNT and Pt@SWNT measured statically. In the same way as the investigation into $Cu(acac)_2$@SWNT, a new sample of $Pt(acac)_2$@SWNT was prepared and held at 175 °C for 1 hr. FD-XAS measurements each took 10 min to complete, and were constantly obtained throughout, with the edge energy monitored as a function of time (figure 18 a). In contrast to $Cu(acac)_2$@SWNT where there was a sharp decrease in the edge energy during the first 10 min, with $Pt(acac)_2$@SWNT, there is a slight decrease in the edge energy over time when held at 175 °C. Additionally, kinetic behaviour can be monitored by examining the value of the edge at 175 °C compared to $Pt(acac)_2$@SWNT at 25 °C and Pt@SWNT formed *ex-situ*. After initially heating the sample, the edge energy suggests a conversion of *ca.* 50%, which slowly increases over time (figure 18 b).

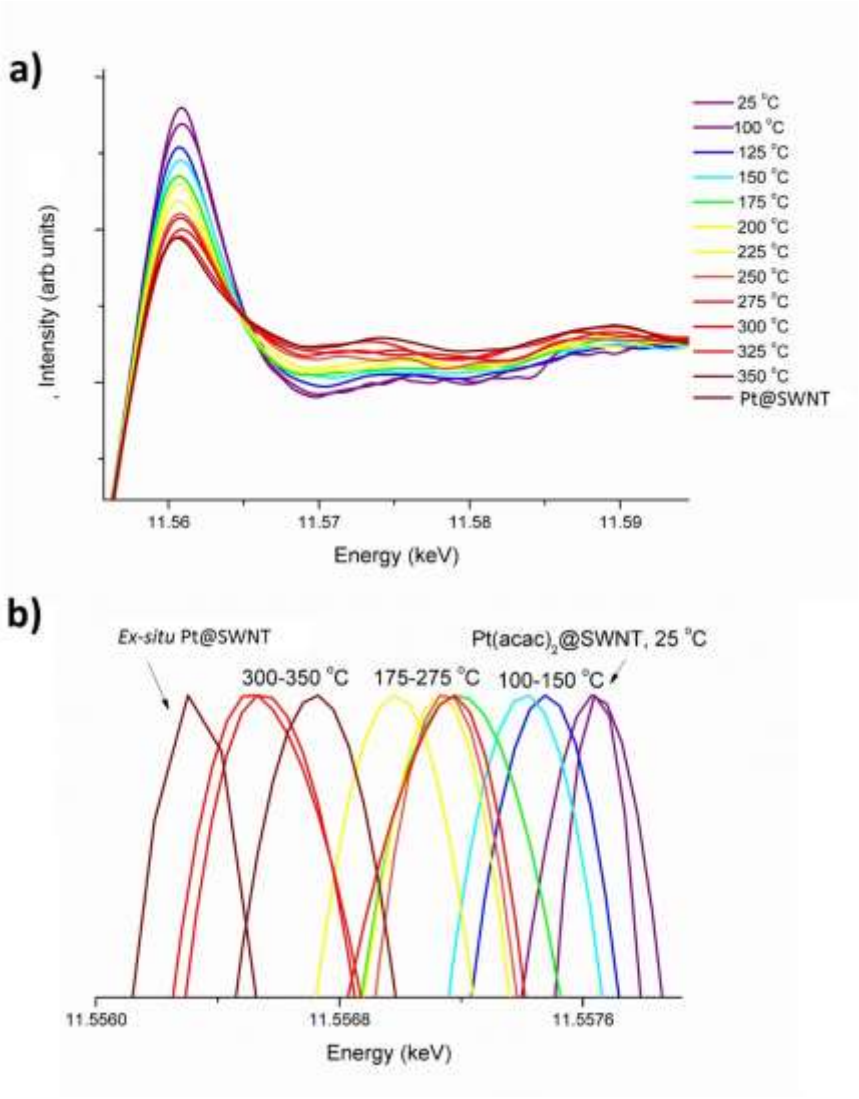

Figure 5.16: The Pt L_{III} edge of FD-XAS spectra of $Pt(acac)_2$@SWNT heated from 100 °C to 350 °C at 25 °C intervals. $Pt(acac)_2$@SWNT at room temperature and Pt@SWNT formed *ex-situ* are shown for comparison. There is a decrease of *ca.* 1 eV in the edge of $Pt(acac)_2$@SWNT upon heating, as shown in the first derivatives of each spectrum (b).

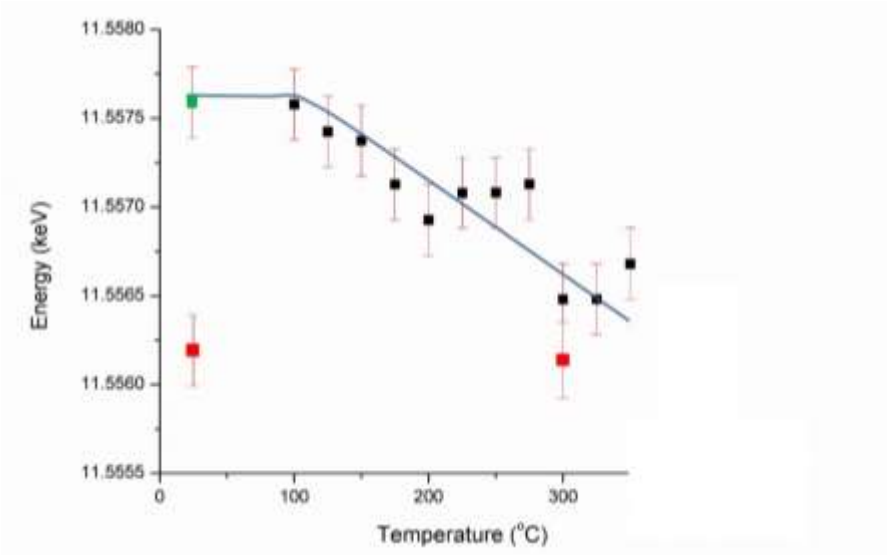

Figure 17: A plot showing how the Pt L_{III} edge of $Pt(acac)_2$@SWNT decreases as a function of temperature. At 100 °C the edge is similar to that of $Pt(acac)_2$@SWNT at room temperature, however with heating the edge decreases. Overall there is a decrease of *ca*. 1.3 eV which is indicative of the platinum L_{III} edge of Pt@SWNT formed *ex-situ*. The edge energies of Pt@SWNT obtained statically at 25 °C and 350 °C are shown for reference (red squares).

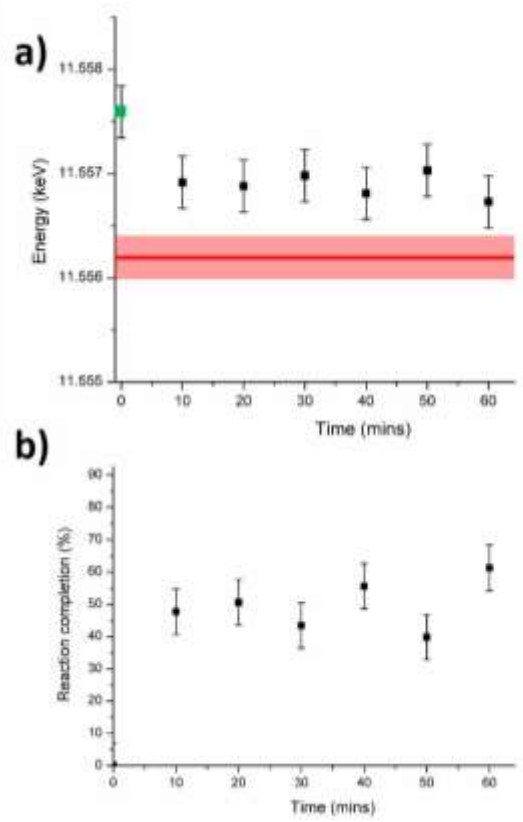

Figure 18: a) A plot showing how the edge energy changes when held at 175 °C for a set amount of time, and compared to $Pt(acac)_2$@SWNT at 25 °C (green square) and Pt@SWNT (red line). There is a slight decrease in the edge energy over time; b) A plot showing how

$Pt(acac)_2$@SWNT to Pt@SWNT as a function of time, as calculated by monitoring the position of the Pt L_{III} edge of the sample at 175 °C.

Similarly to the transformation of $Cu(acac)_2$@SWNT, it has been demonstrated that $Pt(acac)_2$@SWNT can be heated to form a new material, with FD-XAS being an appropriate method to analyse the system *in-situ*. In the same way to copper, the transformation has been showed to occur at a much lower temperature than observed in bulk $Pt(acac)_2$, as free $Pt(acac)_2$ decomposes at around 280 °C.[34] Again, this can be attributed to the polarisation of the Pt-O bond as caused by the nanotube. Unlike the transformation of $Cu(acac)_2$@SWNT to Cu_2O_x@SWNT, the formation of Pt@SWNT from $Pt(acac)_2$@SWNT has a few significant differences, the most striking being that there is only 1.32 eV difference between the edges of encapsulated Pt and $Pt(acac)_2$, compared to 12 eV between $Cu(acac)_2$@SWNT and Cu_2O_x@SWNT but this can be attributed to the nature of the platinum L_{III} edge compared to the copper K edge. Additionally, the transition appears much less defined as there is only a gradual decrease in the edge energy and not a sharp drop around 175 °C which was observed with copper. Unlike the transformation of $Cu(acac)_2$@SWNT, heating $Pt(acac)_2$@SWNT at 175 °C only leads to *ca.* 50% transformation, and even after heating for 1 hr no significant change was observed which shows that a higher temperature is needed to achieve full decomposition.

Formation of an encapsulated PtCu nanowire from ($Pt(acac)_2$+$Cu(acac)_2$)@SWNT.

As well as mono-metallic nanoparticles attracting a lot of interest due to potential future industrial applications, there is a growing interest surrounding binary mixtures of metallic nanoparticles, so-called 'nanoalloys'. These materials are of potential interest as catalysts, for example Au-Ag nanoparticles attached to the surface of SWNTs have been used to capture CO.[31] Furthermore, Pt containing alloys have also been synthesised on a flat surface and have shown to be effective catalysts for the oxidation of methanol.[32] As an extension to the investigation into the transformations of $Cu(acac)_2$@SWNT and $Pt(acac)_2$@SWNT, the synthesis of (PtCu)Nanowires@SWNT has been attempted via the co-encapsulation and subsequent decomposition of $Cu(acac)_2$@SWNT and $Pt(acac)_2$@SWNT. The resultant material has been studied using AC-HRTEM (figure 19).

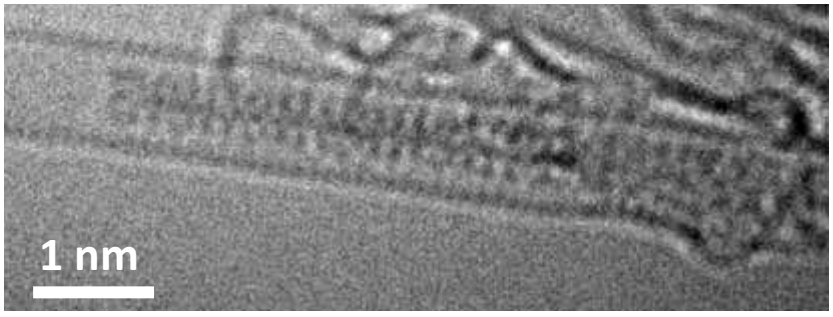

Figure 19: AC-HRTEM image showing Pt_xCu_y@SWNT.

Since the thermal treatment of both $M(acac)_2$@SWNT (M = Pt, Cu) has been investigated using FD-XAFs, monitoring the thermal decomposition of $(Pt(acac)_2+Cu(acac)_2)$@SWNT has also been attempted.

Due to the instrument having to be programmed to a specific energy depending on the edge that is being monitored, the Cu K and Pt L_{III} edges were monitored separately and so different samples of the same material were explored. This avoided any unnecessary time delay between having to switch between each energy when monitoring each edge in tandem. Initially, the Cu K and Pt L_{III} edges were recorded for $(Pt(acac)_2+Cu(acac)_2)$@SWNT at 25 °C, and since 175°C was shown previously as the temperature at which the edges of both M(acac)@SWNT (M=Pt, Cu) changed, the samples were heated up to 175 °C to monitor changes in the energy of the edges over time (figure 20) and the data from each edge was compared to the data of each mono-metallic system.

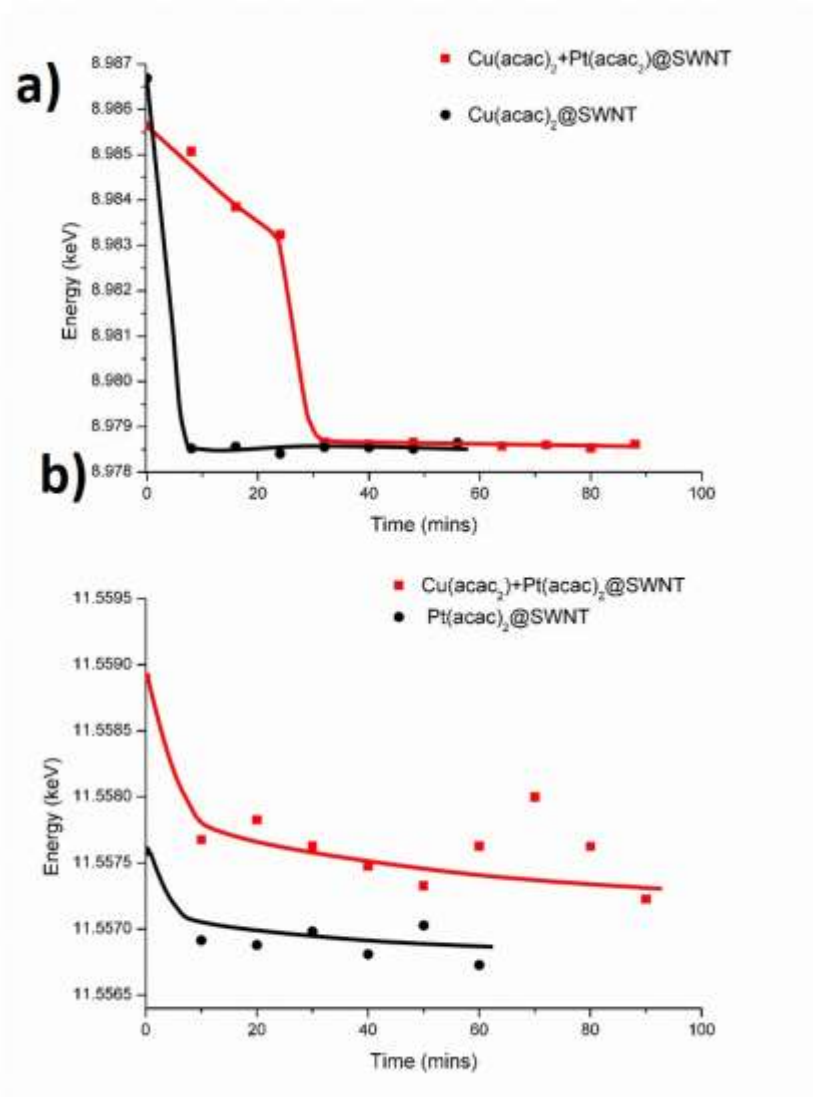

Figure 20: Plots showing how the Cu K edge energy (a) and Pt L_{III} edge energy (b) change when $Cu(acac)_2+Pt(acac)_2$@SWNT is heated at 175 °C for a set amount of time (red lines), compared to the Cu K edge of $Cu(acac)_2$@SWNT (black line, a) and Pt L_{III} edge of $Pt(acac)_2$@SWNT (black line, b).

In contrast to when only $Cu(acac)_2$@SWNT is encapsulated, the addition of $Pt(acac)_2$ to the system appears to slow down the transformation, as a more gradual reduction in the edge energy is observed. This is interesting at is suggests that $Pt(acac)_2$ is inhibiting the formation of Cu_2O_x@SWNT. As a consequence of the delay, the sample was heated for 30 mins longer than that of just $Cu(acac)_2$@SWNT, but whilst the transition occurred at around 25 mins, no further change was observed. Similarly, the thermal decomposition of $Pt(acac)_2$@SWNT appears to be slowed down slightly by the addition of $Cu(acac)_2$ (figure X), but to not as great an extent.

The thermal treatment of ($Pt(acac)_2$+$Cu(acac)_2$)@SWNT proved to be remarkable as a significant decrease in the change of the Cu K edge was observed relative to the monometallic material which is attributed to the formation of a different material, but this system needs to be investigated further. As an extension, *in-situ* Raman heating could also be employed to monitor changes in the G band and provide further quantitative evidence, and AC-HRTEM of all the materials heated at 175 ^oC is required to ensure that these are the same as the materials formed ex-situ, but overall this work has great potential and brings us one step closer to the quest of being able to precisely monitor reactions at the nanoscale.

Conclusion

FD-XAS has been used to monitor how the oxidation state of the metals in both $Pt(acac)_2$@SWNT and $Cu(acac)_2$@SWNT change upon heating. Whilst only preliminary, the results of this investigation provide a solid basis for investigating transformations inside SWNTs, since clear quantifiable trends are shown spectroscopically. The changes in edge energy, and therefore oxidation states of the metal centres occur rapidly, and a majority of both of the materials was converted within the first 10 min at 175 ^oC. This shows a dramatic decrease in the decomposition temperatures of both the acetylacetonate complexes when confined into SWNTs, and can be attributed to polarisation of the M-O bonds which lowers the E_a for bond dissociation. Complimentary use of Raman spectroscopy and FD-XAS supports this hypothesis, as polarisation of the encapsulated complexes upon encapsulation is shown, but no electron transfers to the host nanotube is observed.

In order to fully ascertain whether $Cu(acac)_2$@SWNT heated gradually up to 500 ^oC produces the same material as produced *ex-situ*, detailed AC-HRTEM images of the products formed from *in-situ* heating are required, and monitoring the transformation *in-situ* by Raman could also prove to be enthralling in revealing what has occurred to the sample. Additionally, since the edge energy of $Pt(acac)_2$@SWNT never fully reached the position of Pt@SWNTs, further analysis of this is also required.

It has been shown that the temperature for MNP formation from metallic precursors is much lower than previously thought, which has profound implications on the conditions required to transform materials in nanotubes and could possibly lead to a paradigm shift in the field of nanomaterials synthesis within carbon nanoreactors.

Experimental

Fluorescence-Detected X-ray Absorption Spectroscopy (FD-XAS)

All static-temperature FD-XAS measurements were carried out on the XMaS beamline (BM28) and SpLine (BM25a) at the ESRF. Samples were deposited onto carbon tape, which was then mounted onto a stainless steel sample holder. FD-XAS edge inflection points were obtained by fitting a smoothing spline to the measured spectrum, using Matlab, and taking the first derivative of the fitted spectrum.

In-situ experiments were performed on the SpLine (BM25a) at the ESRF. $M(acac)_2$@SWNT (5 mg) was placed in a glass capillary tube and held in position (figure 5 a.1). The tube was placed within an aluminium frame, sealed, placed in position above a heater (figure 5 a.4) and attached to a helium source (in figure 5 a2, out figure 5 a3, flow rate *ca.* 30 mL/min). Prior to all experiments, the system was purged with helium for 15 min to ensure all air was removed from the capillary tube. Finally, the system was heated rapidly (at a rate of 50 ^{o}C/s) and spectra recorded.

Electron Microscopy

SWNTs filled with the encapsulated materials were dispersed in propan-2-ol using an ultrasonic bath and drop cast onto lacey carbon-coated copper TEM grids (Agar). HR-TEM imaging was carried out on a JEOL 2100 FEG-TEM microscope operated at 200 kV. Aberration-corrected HR-TEM was performed at the University of Ulm on a C_s corrected FEI Titan 80-300 TEM operated at 80 kV with information limit enhancement using reduced extraction voltage.

Raman Spectroscopy

Raman spectroscopy was performed using a HORIBA Jobin Yvon LabRAM HR spectrometer equipped with an automated *xyz* stage (Märzhäuser). Spectra were acquired using a 532 nm laser at 0.2mW power, in the range 50 to 4000 cm^{-1}, with 5 seconds and 8 accumulations per spectral window, using a 50× objective and a 300 µm confocal pinhole. To simultaneously scan a range of Raman shifts, a 600 lines/mm rotatable diffraction grating along a path length of 800 mm was employed. Spectra were detected using a SYNAPSE CCD detector (1024 pixels) thermoelectrically cooled to −60 °C. Before the spectra collection, the instrument was calibrated using the Rayleigh line at 0 cm^{-1} and a standard Si(100) reference band at 520.7 cm^{-1}.

References

1. L. M. de la Rosa-Romo, M. T. Oropeza-Guzman, A. Olivas-Sarabia and G. Pina-Luis, *Sens. Actuator B-Chem.*, 2016, **233**, 459-468.

2. Y. Y. Liang, H. L. Wang, P. Diao, W. Chang, G. S. Hong, Y. G. Li, M. Gong, L. M. Xie, J. G. Zhou, J. Wang, T. Z. Regier, F. Wei and H. J. Dai, *J. Am. Chem. Soc.*, 2012, **134**, 15849-15857.

3. V. M. Aroutiounian, *Lith. J. Phys.*, 2015, **55**, 319-329.

4. S. Palanisamy, H. F. Lee, S. M. Chen and B. Thirumalraj, *RSC Adv.*, 2015, **5**, 105567-105573.

5. V. H. Crespi, N. G. Chopra, M. L. Cohen, A. Zettl and S. G. Louie, *Phys. Rev. B*, 1996, **54**, 5927-5931.

6. T. Susi, J. Kotakoski, R. Arenal, S. Kurasch, H. Jiang, V. Skakalova, O. Stephan, A. V. Krasheninnikov, E. I. Kauppinen, U. Kaiser and J. C. Meyer, *ACS Nano*, 2012, **6**, 8837-8846.

7. J. C. Meyer, F. Eder, S. Kurasch, V. Skakalova, J. Kotakoski, H. J. Park, S. Roth, A. Chuvilin, S. Eyhusen, G. Benner, A. V. Krasheninnikov and U. Kaiser, *Phys. Rev. Lett.*, 2012, **108**.

8. F. Zhang, F. Jiao, X. L. Pan, K. Gao, J. P. Xiao, S. Zhang and X. H. Bao, *ACS Catal.*, 2015, **5**, 1381-1385.

9. D. Friebel, V. Viswanathan, D. J. Miller, T. Anniyev, H. Ogasawara, A. H. Larsen, C. P. O'Grady, J. K. Norskov and A. Nilsson, *J. Am. Chem. Soc.*, 2012, **134**, 9664-9671.

10. H. G. Manyar, R. Morgan, K. Morgan, B. Yang, P. Hu, J. Szlachetko, J. Sa and C. Hardacre, *Catal. Sci. Tech.*, 2013, **3**, 1497-1500.

11. T. Yao, Z. H. Sun, Y. Y. Li, Z. Y. Pan, H. Wei, Y. Xie, M. Nomura, Y. Niwa, W. S. Yan, Z. Y. Wu, Y. Jiang, Q. H. Liu and S. Q. Wei, *J. Am. Chem. Soc.*, 2010, **132**, 7696-7701.

12. J. Ohyama, K. Teramura, T. Shishido, Y. Hitomi, K. Kato, H. Tanida, T. Uruga and T. Tanaka, *Chem. Phys. Lett.*, 2011, **507**, 105-110.

13. F. L. Jiang, C. Li, H. Y. Fu, X. J. Guo, G. Z. Wu and S. M. Chen, *PCCP*, 2016, **18**, 19259-19266.

14. A. A. Eliseev, L. V. Yashina, N. I. Verbitskiy, M. M. Brzhezinskaya, M. V. Kharlamova, M. V. Chernysheva, A. V. Lukashin, N. A. Kiselev, A. S. Kumskov, B. Freitag, A. V. Generalov, A. S. Vinogradov, Y. V. Zubavichus, E. Kleimenov and M. Nachtegaal, *Carbon*, 2012, **50**, 4021-4039.

15. M. V. Kharlamova, M. M. Brzhezinskay, A. S. Vinogradov, I. P. Suzdalev, Y. V. Maksimov, V. K. Imshennik, S. V. Novichikhin, A. V. Krestinin, L. V. Yashina, A. V. Lukashin, Y. D. Tret'yakov and A. A. Eliseev, *Nanotechnol. Russ.*, 2009, **4**, 634.

16. N. Thamavaranukup, H. A. Hoppe, L. Ruiz-Gonzalez, P. Costa, J. Sloan, A. Kirkland and M. L. H. Green, *Chem. Commun.*, 2004, 1686-1687.

17. K. Yanagi, Y. Miyata and H. Kataura, *Adv. Mater.*, 2006, **18**, 437-441.

18. A. Chuvilin, E. Bichoutskaia, M. C. Gimenez-Lopez, T. W. Chamberlain, G. A. Rance, N. Kuganathan, J. Biskupek, U. Kaiser and A. N. Khlobystov, *Nat. Mater.*, 2011, **10**, 687-692.

19. T. W. Chamberlain, T. Zoberbier, J. Biskupek, A. Botos, U. Kaiser and A. N. Khlobystov, *Chem. Sci.*, 2012, **3**, 1919-1924.

20. T. Zoberbier, T. W. Chamberlain, J. Biskupek, N. Kuganathan, S. Eyhusen, E. Bichoutskaia, U. Kaiser and A. N. Khlobystov, *J. Am. Chem. Soc.*, 2012, **134**, 3073-3079.

21. I. V. Lebedeva, T. W. Chamberlain, A. M. Popov, A. A. Knizhnik, T. Zoberbier, J. Biskupek, U. Kaiser and A. N. Khlobystov, *Nanoscale*, 2014, **6**, 14877-14890.

22. S. J. Guo, X. L. Pan, H. L. Gao, Z. Q. Yang, J. J. Zhao and X. H. Bao, *Chem. Eur. J.*, 2010, **16**, 5379-5384.

23. L. M. Zhang, Z. B. Wang, J. J. Zhang, X. L. Sui, L. Zhao and D. M. Gu, *Carbon*, 2015, **93**, 1050-1058.

24. L. Grigorian, K. A. Williams, S. Fang, G. U. Sumanasekera, A. L. Loper, E. C. Dickey, S. J. Pennycook and P. C. Eklund, *Phys. Rev. Lett.*, 1998, **80**, 5560-5563.

25. A. Botos, J. Biskupek, T. W. Chamberlain, G. A. Rance, C. T. Stoppiello, J. Sloan, Z. Liu, K. Suenaga, U. Kaiser and A. N. Khlobystov, *J. Am. Chem. Soc.*, 2016, **138**, 8175-8183.

26. A. G. Nasibulin, P. P. Ahonen, O. Richard, E. I. Kauppinen and I. S. Altman, *J. Nanopart. Res.*, 2001, **3**, 385-400.

27. T. S. Koblenz, J. Wassenaar and J. N. H. Reek, *Chem. Soc. Rev.*, 2008, **37**, 247-262.

28. S. A. Miners, G. A. Rance and A. N. Khlobystov, *Chem. Soc. Rev.*, 2016, **45**, 4727-4746.

29. J. B. Raoof, S. R. Hosseini and S. Rezaee, *J. Mol. Liq.*, 2015, **212**, 767-774.

30. Z. L. Liu, L. M. Gan, L. Hong, W. X. Chen and J. Y. Lee, *J. Power Sources*, 2005, **139**, 73-78.

31. D. Zhai, B. Liu, Y. Shi, L. Pan, Y. Wang, W. Li, R. Zhang and G. Yu, *ACS Nano*, 2013, **7**, 3540-3546.

32. R. Nakanishi, R. Kitaura, P. Ayala, H. Shiozawa, K. de Blauwe, P. Hoffmann, D. Choi, Y. Miyata, T. Pichler and H. Shinohara, *Phys. Rev. B*, 2012, **86**.

33. P. Ayala, R. Kitaura, R. Nakanishi, H. Shiozawa, D. Ogawa, P. Hoffmann, H. Shinohara and T. Pichler, *Phys. Rev. B*, 2011, **83**, 085407.

34. S. Flanagan, E. Hall, W. Bowie, J. W. Fuhs, R. Logan, F. Maniei and A. Hunt, *Green Chem.*, 2005, **7**, 333-338.